iScience

CellPress
OPEN ACCESS

Article

Development of chimeric antigen receptor (CAR)-T cells targeting A56 viral protein implanted by oncolytic virus

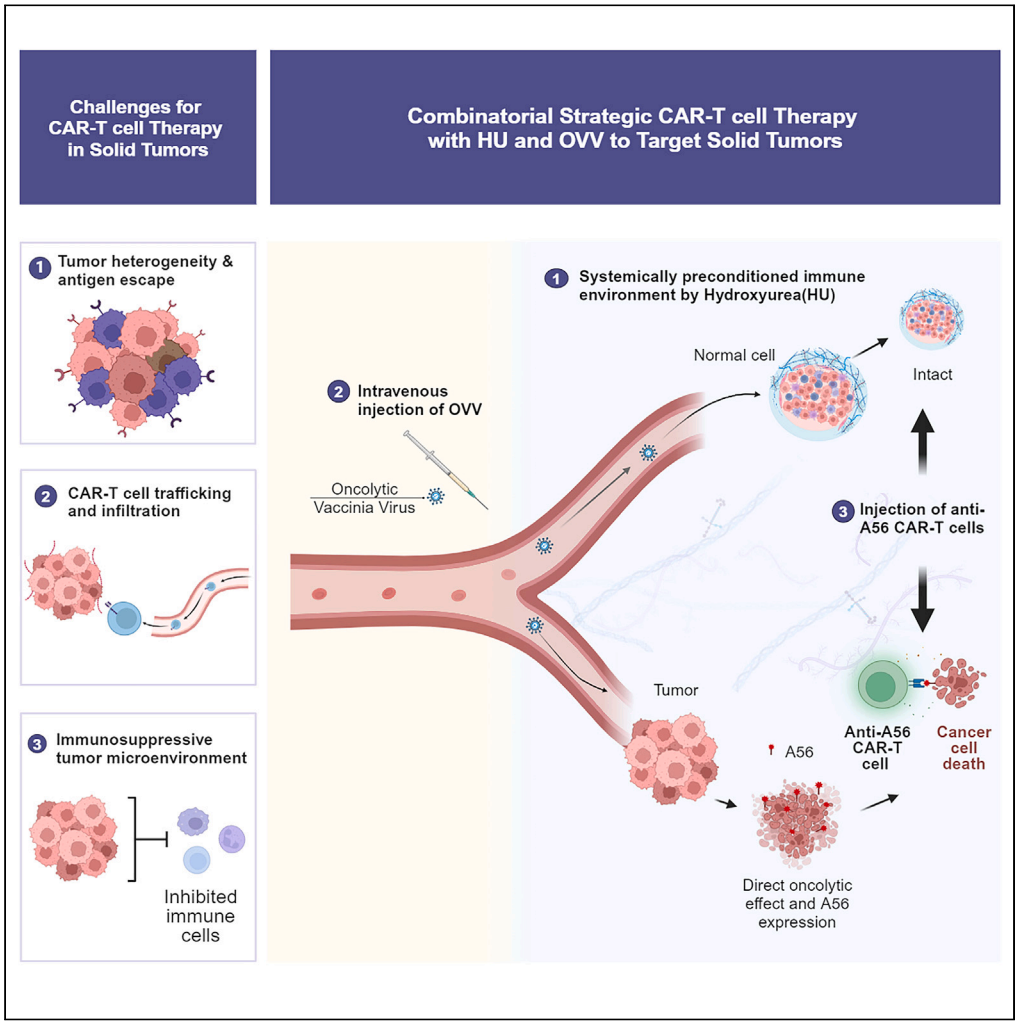

Euna Cho, Min Ho An, Yi Sle Lee, ..., Young Mi Hong, Mong Cho, Tae Ho Hwang

thhwang@pusan.ac.kr

Highlights

A56 persisted as a targetable membrane protein after infection of oncolytic virus

A56 CAR-T showed A56-dependent cytotoxicity *in vitro*

A56 CAR-T with OV/hydroxyurea treatment enhanced anti-tumor effect in mice

Cho et al., iScience 27, 109256
March 15, 2024
https://doi.org/10.1016/j.isci.2024.109256

iScience

CellPress
OPEN ACCESS

Article

Development of chimeric antigen receptor (CAR)-T cells targeting A56 viral protein implanted by oncolytic virus

Euna Cho,[1,10] Min Ho An,[2,3,10] Yi Sle Lee,[1] Eun Jin Ryu,[1] You Ra Lee,[1] So Youn Park,[1] Ye Ji Kim,[1] Chan Hee Lee,[1] Dayoung Oh,[1] Min Seo Kim,[4] Nam Deuk Kim,[5] Jae-Joon Kim,[6] Young Mi Hong,[7] Mong Cho,[1] and Tae Ho Hwang[1,8,9,11,*]

SUMMARY

To address the challenge of solid tumor targeting in CAR-T therapy, we utilized the A56 antigen, which is uniquely expressed on a diverse range of cancer cells following the systemic administration of an oncolytic vaccinia virus (OVV). Immunohistochemical assays precisely confirmed exclusive localization of A56 to tumor tissues. *In vitro* studies demonstrated a distinct superiority of A56-dependent CAR-T cytotoxicity across multiple cancer cell lines. Building on these *in vitro* observations, we strategically administered A56 CAR-T cells, OVV, and hydroxyurea (HU) combination in HCT-116 tumor-bearing non-obese diabetic/severe combined immunodeficiency (NOD/SCID) mice, leading to a significant reduction in tumor size and an extended time to progression. Consequently, A56-targeting combinatorial immunotherapy provides the benefit of reducing inadvertent CAR-T effects on normal cells while preserving its effectiveness against cancer cells. Furthermore, our approach of implanting A56 via OVV on tumors facilitates a wide therapeutic application of CAR-T cells across various solid tumors.

INTRODUCTION

The advent of chimeric antigen receptor (CAR)-T cell has changed the treatment landscape for hematologic malignancies, offering substantial benefits in terms of response rates for diseases such as leukemia,[1,2] lymphoma,[3,4] and multiple myeloma.[5,6] However, the response rates of CAR-T were not as satisfactory in solid tumors,[7,8] attributable to various interwind factors such as minimal CAR-T cell trafficking into the solid tumor, immunosuppressive tumor microenvironment (TME), and tumor antigen heterogeneity.[9,10] Among those factors, a major challenge resides in the lack of specific target antigens that are truly confined to solid tumors. The CAR-T therapy raises significant safety issues in the absence of such limited expression and subsequently narrows the therapeutic window in solid tumor.[11]

Numerous clinical trials have documented serious toxicities caused by off-tumor antigen (in normal tissue) recognition by CAR-T cells for solid tumors.[12,13] To increase selectivity and minimize the safety risk, CAR-T therapy combined with an oncolytic virus (OV) was proposed as a promising strategy for solid tumors.[14,15] The engineered viruses promote tumor selectivity for direct oncolysis, introduce immune-stimulating effect to combat immunosuppressive TME,[16] and express cytokines to recruit T cells and further enhance anti-tumor immunity.[17]

The recent study by Park et al. explored the strategy using OV to deliver non-signaling truncated CD19 to the membrane of solid tumors paired with CD19-targeting CAR-T cell and confirmed its effectiveness.[18] Although the proof-of-concept for combining truncated CD19-OV with CD19-targeting CAR-T cell for solid tumor was a breakthrough, safety concerns persist as CD19 is known to be expressed in normal tissues.

In the current study, we capitalized on the non-signaling viral antigen A56.[19–21] Upon infection with the oncolytic vaccinia virus OTS-412, this antigen is homogeneously expressed on the plasma membrane of the infected tumor cells. The distinct feature of this protein within the

[1]Research Center, Bionoxx Inc., Seongnam-si, Gyeonggi-do 13554, Republic of Korea
[2]Department of Biomedical Informatics, Ajou University School of Medicine, Suwon, Republic of Korea
[3]Department of Medical Sciences, Graduate School of Ajou University, Suwon, Republic of Korea
[4]Samsung Advanced Institute for Health Sciences & Technology (SAIHST), Sungkyunkwan University, Samsung Medical Center, Seoul 06351, Republic of Korea
[5]Department of Pharmacy and Pusan Cancer Research Center, Pusan National University, Busan 46241, Republic of Korea
[6]Oncology and Hematology Clinic, Department of Internal Medicine, Pusan National University Yangsan Hospital, Yangsan 50612, Republic of Korea
[7]Liver Center, Pusan National University Yangsan Hospital, Department of Internal Medicine, School of Medicine, Pusan National University, Yangsan 50612, Republic of Korea
[8]Medical Research Center, School of Medicine, Pusan National University, Yangsan 50612, Republic of Korea
[9]Department of Pharmacology, School of Medicine, Pusan National University, Yangsan 50612, Republic of Korea
[10]These authors contributed equally
[11]Lead contact
*Correspondence: thhwang@pusan.ac.kr
https://doi.org/10.1016/j.isci.2024.109256

field of CAR-T therapy also lies in its non-human origin, making it a potentially viable target antigen. Given these attributes, we propose that A56 could serve as a tumor-specific antigen, broadly applicable across a diverse range of solid tumors permissive to OTS-412.

In addition to using the oncolytic vaccinia virus (OVV) to deliver targetable antigens, this study incorporates a combinatorial approach with hydroxyurea (HU). HU, recognized as a ribonucleotide reductase inhibitor,[22] was selected based on our prior findings that demonstrated the presence of neutrophils could diminish the cytotoxicity of OVV against cancer cells (Figures S1A and S1B). Additionally, our subsequent comparative analysis on various immune-modulating agents revealed that the combination of HU with OVV exhibited the most significant synergistic anti-tumor effect (Figures S1C and S1D). Although the exact mechanism has not been fully elucidated, neutrophils are suspected to play a role in modulating the immune environment and HU may potentially enhance the anti-tumor activity of OVV given that HU is known to suppress granulopoiesis.[22] While concurrent research is underway to further investigate the interactions among neutrophils, the host immunity, and OVV against cancer cells, this study primarily aims to assess the delivery of A56 antigens via OVV and the subsequent CAR-T therapy following the combined treatment with OVV and HU, serving as an adjunctive therapeutic approach.

In our proof-of-concept study, we thereby hypothesized that the combination of A56 CAR-T cells following OVV/HU treatment could increase the potency of OVV and may avoid the risks of off-target effects inherent to CAR-T cell therapy by delivering a non-human antigen via an OVV with enhanced specificity to tumor cells.

RESULTS

Homogenous expression of A56 following OVV treatment and essential domains for A56 localization on the plasma membrane of tumor cells

To evaluate the tumor-targeting potential of A56, we infected A549 cancer cells with a GFP expressing-OVV. Immunofluorescence images showed that A56-positive fluorescence was localized on the outer plasma membrane of infected cancer cells (Figure 1A). To investigate the structural elements involved in A56 localization on the plasma membrane, we generated four different A56 constructs, three of which lacked specific domains (Figure 1B). When transduced into U2-OS cells, only the full A56-GFP sequence vector demonstrated plasma membrane localization of the A56 protein without aggregation or retention within the Golgi or endoplasmic reticulum (ER) (Figure 1C).

Consistent A56 expression on the plasma membrane of cancer cells across varied virus concentrations and time points

To determine the expression of A56 and cell viability upon direct viral oncolysis at different multiplicity of infection(MOI)s and time points, three human cell lines derived from different organs were treated with OTS-412 virus at MOIs ranging from 0.0125 to 1. Subsequently, A56 expression and cell viability were quantified at 2, 24, and 48 h post-infection using flow cytometry (Figure S2). Elevated expression levels of A56 were observed with an increase in MOI at the 2 and 24 h time points, accompanied by minor differences in cell viability across the three cell lines. Moreover, the proportion of A56 expression on the surface of cell plasma membrane remained consistent across these observations, indicating the antigenic potential of A56 to be targeted by CAR-T. Notably, at the 48 h time point, a more pronounced increase in A56 expression was observed in non-viable cells relative to viable cells when subjected to higher MOIs, which is attributable to cell lysis.

A56 expression on the plasma membrane surface *in vitro* and *in vivo* after systemic injection of OTS-412 in a tumor bearing xenograft mouse model

Given the extracellular expression of A56 observed previously, the possibility of intracellular A56 expression was evaluated using flow cytometry. Intracellular A56 expression was nearly undetectable across all examined time points and MOI levels (Figure 2A). A56 expression was further confirmed *in vivo* by intravenous injection of OTS-412 into HT-29 tumor-bearing non-obese diabetic/severe combined immunodeficiency (NOD/SCID) mice. OTS-412 is a recombinant oncolytic vaccinia virus in which the VV-tk gene (thymidine kinase) has been replaced with an HSV-tk (herpes simplex virus thymidine kinase). This virus has demonstrated comparable cytotoxicity to a VV-tk gene-deleted vaccinia virus in various cancer cell lines, both *in vitro* and *in vivo*, while incorporating safety mechanisms to control undesired viral replication.[23] The immunofluorescence analysis exhibited distinct localization of two viral proteins (A56 and A27L); A56 protein was homogeneously expressed on the cell surface of the tumor tissue whereas A27L was expressed in the cytosol (Figure 2B).

Selective and persistent A56 expression in tumor tissue following OTS-412 and hydroxyurea treatment in a New Zealand white rabbit model

Since the replication of Wyeth strain-based vaccinia virus is limited in mouse models,[24–26] the virus permissive New Zealand White rabbit model was chosen to assess the virus and A56 distribution. VX2 tumor-bearing rabbits were treated with OTS-412 alone or in combination with HU, and then A56 expression was evaluated in the organ and tumor tissues using immunofluorescence (Figure 2C) and quantified (Figure 2D). Remarkably, the combination treatment of OTS-412 and HU resulted in cancer-selective expression of A56, while OTS-412 alone showed non-specific distribution in some organ tissues on day 5 prior to viral clearance. The tumor-selective replication of OTS-412 with hydroxyurea combination was maintained until day 28. To assess the tumor selectivity of the virus and the relationship between viral persistence and A56 expression, viral copies of OTS-412 from the OTS-412/HU combination treatment group were quantified as well (Figure 2E). The viral copy number in the tumor tissue reached its peak on day 14 and was detectable until day 28. More importantly, A56 expression persisted until day 28.

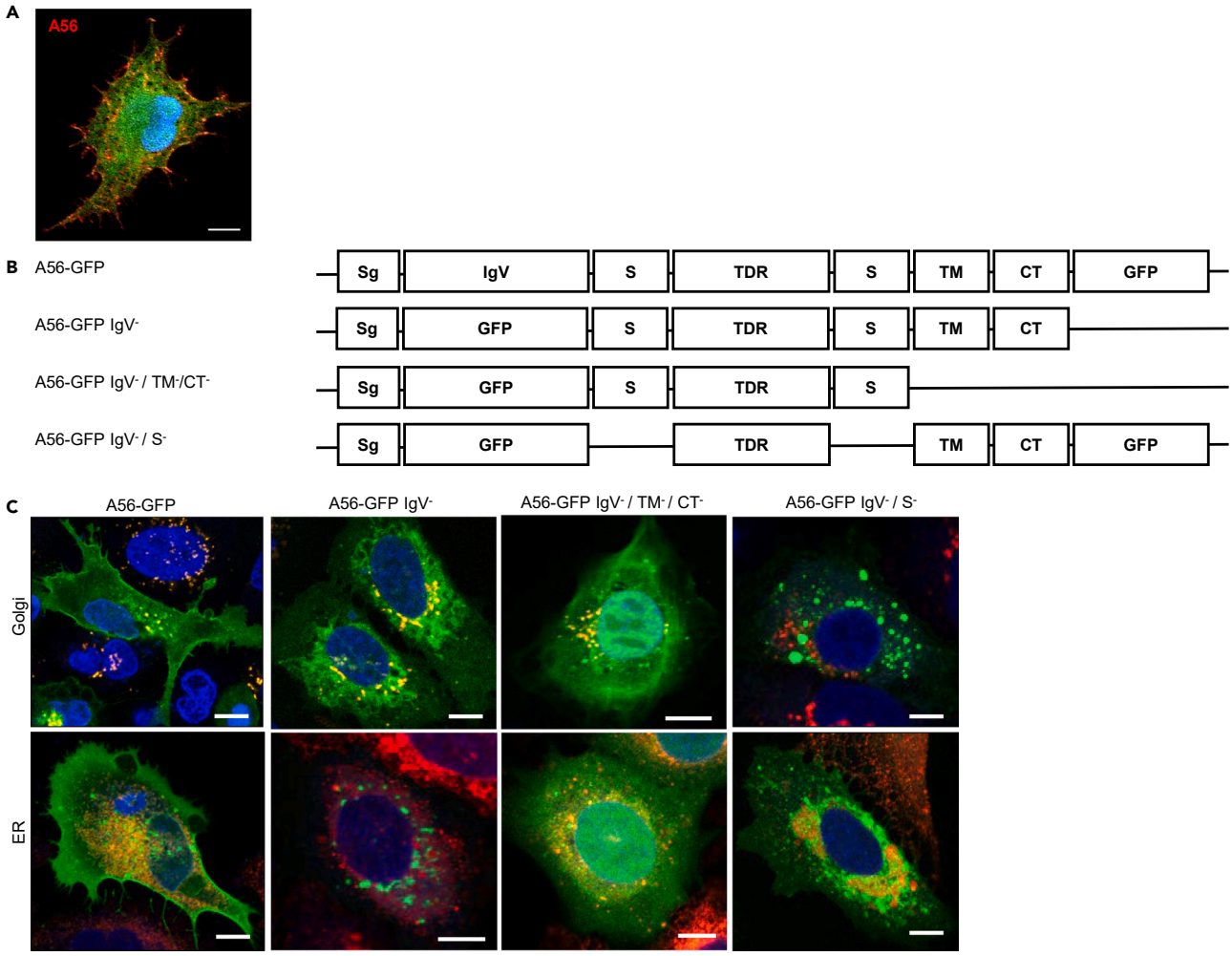

Figure 1. Essential domain of A56 for its localization on cell plasma membrane

(A) Confocal immunofluorescence (IF) microscopy of OVV-infected A549 tumor cells showing A56 expression; nuclei (blue), OVV (green), A56 (red); scale bar, 10 μm.

(B) Full A56 construct design compared with those of various A56 mutant constructs that do not have one or more domains; Sg, signaling domain; IgV, IgV-like domain; TDR, tandem repeat domain; S, stalk region; TM, transmembrane domain; CT, cytoplasmic tail.

(C) Merged confocal images of A56 localization on the plasma membranes of U2-OS tumor cells upon full A56-expressing plasmid transduction compared to proteins enclosed within the Golgi or ER from transduction with mutant A56 vectors; nuclei (blue), A56 (green), Golgi apparatus or endoplasmic reticulum (red); scale bar, 10 μm.

The dose and time-dependent A56 expression in tumors following systemic oncolytic virus treatment

To examine the impact of different doses of OVV and the subsequent time-dependent A56 coverage in tumors, NOD/SCID mice bearing HCT-116 tumors were treated with OTS-412 in combination with HU. Immunohistochemistry analysis was performed with tumor and organ tissues on day 3, 7, 10, and 14 (Figure S3A), and A56 expression was quantified (Figure S3B). Consistent with the distribution and duration of A56 observed in the rabbit model, A56 was prominently and uniformly detected on the cellular surface of tumor tissues following the injection of 1×10^6 plaque-forming units (pfu) and 1×10^5 pfu into mice on day 14. A56 expression was only observed in the tumor tissue for all time points. While A56 was not discernible in tumor tissue at the low viral dose on day 10, A56 expression was observed irrespective of the viral dose on day 14, further supporting the durability of A56 expression. Hence, CAR-T cells can be administered within the time frame of A56 expression and can be managed by adjusting the viral dose or considering time elapsed since virus injection. Having confirmed the persistent tumor-selective expression of A56 *in vivo*, we subsequently developed a CAR construct incorporating the anti-A56 single-chain variable fragment (scFv) sequence.

Appropriate CAR screening and development of anti-A56 CAR-T cells

To develop a specific and potent CAR construct, functional anti-A56 VH/VL sequences were identified by bio-panning of a human cDNA phage display library and using *de novo* sequencing of a commercially available anti-A56 antibody derived from mice (Figure S4A). Through

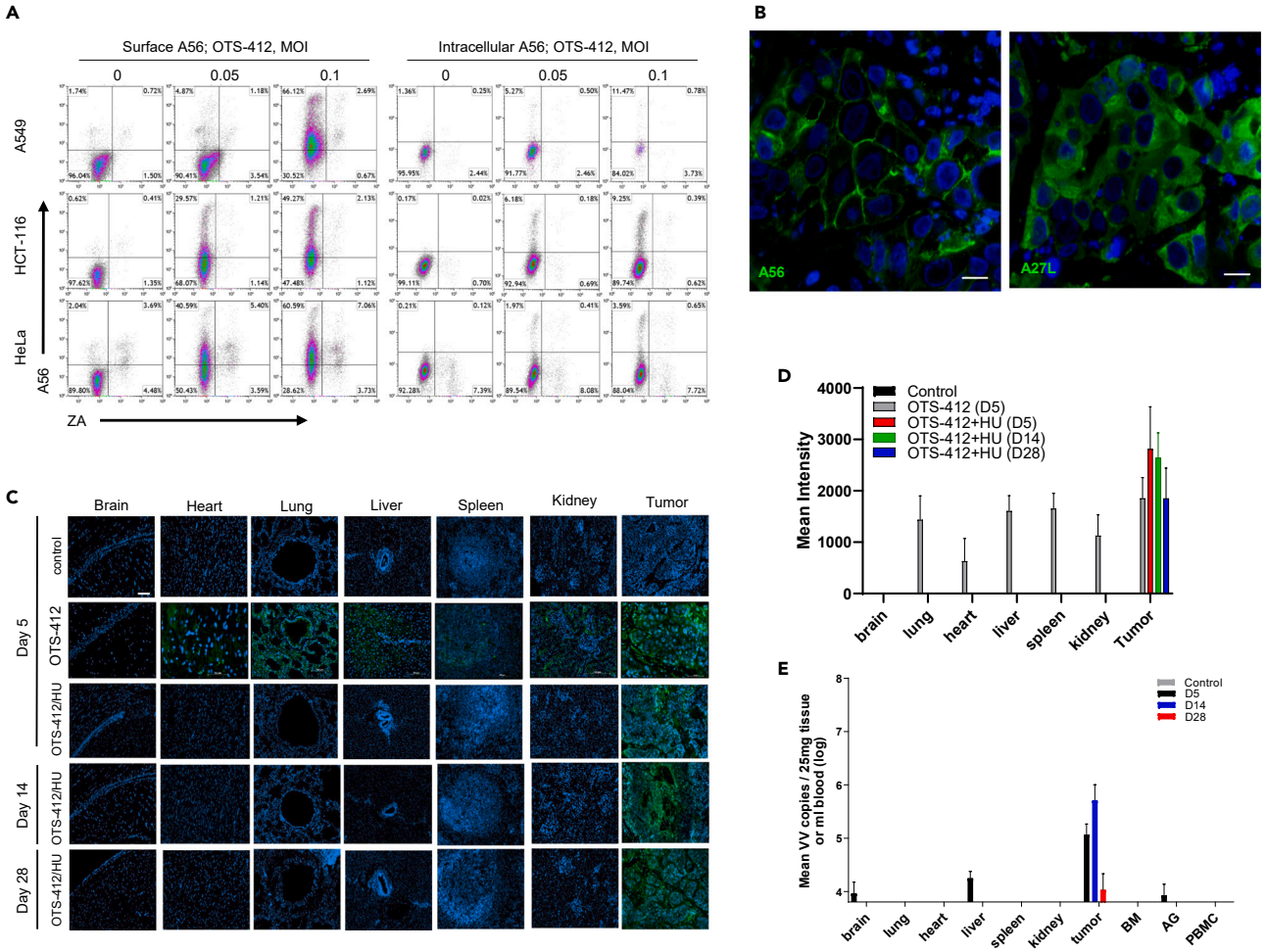

Figure 2. Localization of A56 on solid tumor plasma membrane and distribution in tumor tissue

(A) OTS-412 were treated in A549, HCT-116, HeLa cancer cells at 0.05 and 0.1 MOI for 24 h followed by detection of A56 expression via flow cytometry. Dead cells were excluded by Zombie Aqua (ZA) staining. For intracellular detection of A56, fixation/permeabilization was performed before anti-A56 staining.

(B) Analysis of A56 expression compared to A27L (a vaccinia virus cytosolic protein) expression on tumor tissue collected 4 days post-OV injection of HT-29 tumor-bearing mice. Scale bar, 100 px (=438 μm).

(C) IF analysis of tumor-specific A56 expression and non-expression on other tissues from VX2 tumor-bearing New Zealand White rabbits collected on day (D) 5, 14, and 28 after intravenous injection of OTS-412/HU; The data shown are representative of six and two individual rabbits from the treatment and control groups, respectively. Scale bar, 200 μm.

(D) Quantitation of A56 expression detected from each tissue of Figure 2C presented in mean intensity of fluorescence. Data are represented as mean ± SEM.

(E) Distribution of OTS-412 in the OTS-412/HU combination group presented in mean viral copies per 25 mg of each tissue and 1 mL of PBMC analyzed until D28 post virus injection. Data are represented as mean ± SEM. BM; bone marrow, AG; adrenal gland.

this process, 61 candidates were screened from the final VH/VL sequences derived from the human library. From this pool, five VH/VL sequences were selected based on their binding affinity (Kd < 10^{-9} M as confirmed by biolayer interferometry). Subsequently, these selected VH/VL sequences were transduced as part of single-chain variable fragments (scFvs) to generate A56-targeting CAR-T cells. Among the five candidates, the Hu Ab16 scFv was chosen based on its high transduction rate (>50%) and notable cytotoxicity (Figures S4B and S4C). Most importantly, Hu Ab16 CAR (referred to as A56 CAR in this study) did not demonstrate binding with the five human-derived cell lines tested (Figure S4D) without OTS-412 treatment suggesting no cross-reactivity with human endogenous molecules. Next, we compared the proportion of $CD25^+$ expression in UTD-T cells and A56 CAR-T cells across four cancer cell lines treated with OTS-412. The data, as depicted in Figure S4E, indicated a notable increase in the percentage of $CD3^+/CD25^+$ CAR-T cells in the presence of A56 compared to that of UTD.

Additionally, two functional scFvs, namely Mo Ab01 and Mo Ab02, were obtained through *de novo* sequencing. CAR constructs with Hu Ab16, Mo Ab01, and Mo Ab02 scFvs were all engineered as second-generation CAR-T cells featuring 41BB and CD3ζ domains. The antigen-binding site characteristics and cytotoxicity of Hu Ab16 CAR-T cells were compared to those of the CAR-T cell candidates from *de novo* sequencing (Figures S5A and S5B). The epitopes recognized by all three scFvs showed non-linear characteristics and were mutually distinct

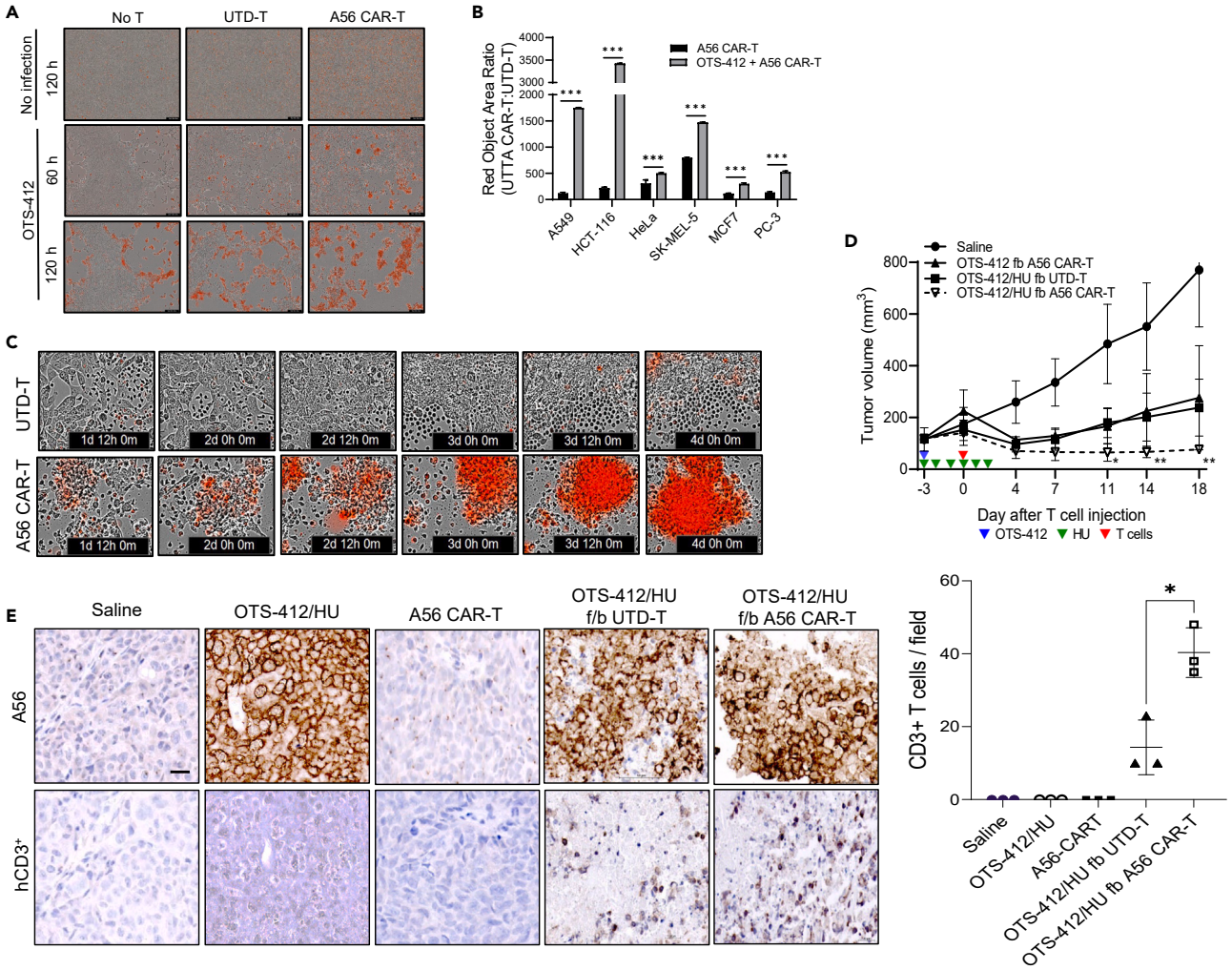

Figure 3. *In vitro* and *in vivo* functionality of A56-specific A56 CAR-T cells

(A) Real-time cytotoxicity of A56 CAR-T cells against HCT-116 cells infected with 0.05 MOI of OTS-412.

(B) Quantification of A56 CAR-T cell cytotoxicity in various human cancer cell lines infected with OTS-412. (***$p < 0.001$, comparison of T cell groups; n = 2 for A549, HCT-116, HeLa, SK-MEL-5 and n = 3 for MCF7 and PC-3 by two-tailed unpaired t test). Data are represented as the mean value ± SEM.

(C) Aggregation of A56 CAR-T cells targeting tumor cells observed every 12 h until day 4 in real-time.

(D) Antigen-dependent anti-tumor efficacy of A56 CAR-T cells in HCT-116 tumor-bearing mice after intratumoral T cell injection following OTS-412 injection with or without HU (*$p < 0.05$, **$p < 0.01$, comparison of T cell groups; saline, n = 5; treatment groups, n = 4, two-way ANOVA with multiple comparison). Data are represented as the mean value ± SD.

(E) IHC analysis of A56 expression and infiltrated hCD3$^+$ T cells in tumors isolated from HCT-116 tumor-bearing mice 21 days post-intravenous T cell treatment. Scale bar, 20 μm (left panel) and quantitation of tumor-infiltrating A56 CAR-T cells positive for hCD3 (right panel) (*$p = 0.01$, n = 3, two-tailed unpaired t test). Data are presented as the mean ± SD. MOI, multiplicity of infection; IHC, immunohistochemistry.

from one another. Notably, Hu Ab16 CAR-T cells exhibited significantly greater cytotoxicity compared to the two CAR constructs derived from mice.

A56 CAR-T cells exhibit antigen-specific cytotoxicity in various cell lines, characterized by prominent aggregation

We investigated the antigen-specific efficacy of A56 CAR-T cells against A56, delivered by OTS-412 *in vitro*. To measure cytotoxicity, we assessed tumor cell lysis in various cancer cells infected with OTS-412. Real-time imaging using Cytotox Red, a dye that detects cell death, was employed to visualize the tumor cell-killing ability of A56 CAR-T cells in the OTS-412-infected HCT-116 cancer cell line. The representative image in Figure 3A demonstrates a higher cancer cell-killing capability of A56 CAR-T cells in HCT-116 infected with OTS-412 at an MOI of 0.05 compared to un-transduced (UTD) T cells. This marked difference was consistently observed across various cancer cell lines (Figure 3B).

A56 CAR-T cells exhibited significantly greater HCT-116 cancer cell lysis in a time-dependent manner when compared to UTD-T cells. This cytotoxicity was accompanied by a higher number of aggregated A56 CAR-T cells and larger aggregation areas observed *in vitro* (Figure 3C). While UTD-T cells induced a certain level of cell death, noticeable cell aggregation was scarcely observed. As a result, tumor cell growth remained largely unaffected. In contrast, A56 CAR-T cells demonstrated a more pronounced ability to encapsulate dividing tumor cells and effectively eliminate them at a rate surpassing their own rate of growth. This enhanced efficacy was visualized by the substantial expansion of the red objective area (Video S1).

Antigen-specific anti-tumor effects of A56 CAR-T cells following OTS-412/hydroxyurea combination treatment in a mouse model

Encouraged by the observed cytotoxicity of A56 CAR-T cells following OTS-412 treatment, we sought to investigate the anti-tumor efficacy of A56 CAR-T cells *in vivo*. Considering our previous findings indicating improved anti-tumor potency of OTS-412 with HU combination treatment (Figure S1C), we employed the OTS-412/HU combination therapy to enhance A56 expression in tumor tissues.

In this study, HCT-116 tumor-bearing NOD/SCID mice were subjected to OTS-412/HU treatment, followed by intra-tumoral (IT) injection of A56 CAR-T cells (Figure 3D). Remarkably, while all groups receiving OTS-412 showed significant reduction in tumor volume, the group treated with A56 CAR-T cells following OTS-412/HU demonstrated the greatest reduction in tumor volume, which was sustained until the end of the observation period (day 18), in contrast to the other groups where tumor volume subsequently increased. To further evaluate the impact of our treatment strategy on tumor growth, we performed intravenous (IV) injection of A56 CAR-T cells following OTS-412/HU combination. The group that received A56 CAR-T cells following OTS-412/HU combination exhibited a significantly greater reduction in tumor volume from day 11 compared to the group treated with OTS-412/HU (Figure S6A). Moreover, a significant delay in time-to-progression was observed in the group treated with A56 CAR-T cells following OTS-412/HU combination compared to the group treated with OTS-412/HU (Figure S6B).

Lastly, evaluation on the human $CD3^+$ infiltration in tumor tissue was performed. Tumor tissue of mice euthanized on day 21 post-CAR-T cell treatment was stained for A56 and human CD3 (Figure 3E). The proportion of infiltrated $hCD3^+$ T cells was significantly highest in the group treated with A56 CAR-T following OTS-412/HU.

DISCUSSION

We explored a non-human viral protein, A56, which is expressed on the tumor cell membrane upon infection by an OVV. Furthermore, we developed a CAR construct that specifically targets the A56 protein expressed on the tumor cell membrane. Our study demonstrated a potent anti-tumor response, achieved through a combined treatment strategy that utilized an oncolytic vaccinia virus, A56-targeting CAR T cells, and HU. This integrated therapeutic approach proved effective not only in *in vitro* studies but also *in vivo*, thereby emphasizing its potential applicability in cancer treatment.

In this study, homogenous expression of the A56 on the plasma membrane of tumor cells and tissues was observed in our study (Figures 1 and 2). A56, a protein with a molecular weight of 34.7 kDa, is heavily glycosylated and highly conserved among different strains of the vaccinia virus and across the poxvirus family. In contrast, it does not have any sequence homology with any other non-human or human endogenous proteins. Despite few reports of its supportive role in virus virulence as a supra-infection inhibitor[20] or a modulator of NK activity,[27] even fewer reports describe its immunogenicity[28,29] that may have direct consequences to A56 CAR-T cell efficacy or safety. Although Johnson et al.[28] and Putz et al.[30] observed humoral immune response induced against A56 in serum after treatment with vaccinia virus-based smallpox vaccine; a vaccinia virus proteome screening of binding with rhesus macaque MHC1 allele by Walsh et al.[29] did not report of cellular response against A56. As inflammatory cytokines induced by supra-activation of $CD8^+$ T cells are one of the primary mechanisms behind CAR-T cell cytotoxicity,[31] A56 may not play a discerning role in inducing a severe immunogenic response, though in-depth cross-reactivity studies are warranted. Additionally, due to the limited replication of Wyeth strain-based vaccinia virus in mouse models, we employed a rabbit model to examine the distribution of the virus and A56 (Figures 2C–2E). Although a minimal number of viral copies were detected in normal organs solely on day 5 (Figure 2E), A56 expression was absent on all days examined. Notably, the combined treatment of OTS-412 and HU resulted in enhanced selective expression of A56 in tumor tissue until day 28. Despite a decrease in detectable viral copies, the persistent expression of A56 was maintained (Figures 2C and 2D). These findings suggest that A56 retains its targetability even after substantial reduction of the virus in tumor tissues.

Furthermore, we discovered that the concomitant administration of HU with OTS-412 amplified the density of A56 and enhanced the selectivity of the virus toward tumor cells. We also documented the additional anti-tumoral activity of A56 CAR-T cells post-OVV infection *in vitro*. Our study highlighted notable T cell aggregation (Figure 3C and Video S1), a phenomenon previously suggested to predict effective T cell cytotoxicity against tumor cells *in vivo*.[32,33] Aggregation of T cells was reported to enhance T cell stimulation correlating with *in vivo* efficacy.[22,34] High degree of aggregation may indicate the formation of strong immune synapses via the interaction of A56 with A56 CAR-T cells. Such aggregation could also amplify T cell functionality through cell-to-cell interactions, further leading to secondary T cell activation and proliferation.[35,36]

Moreover, our results showed that the inclusion of HU significantly reduced tumor volume during A56 CAR-T cell treatment following OTS-412 administration compared with controls and A56 CAR-T treatment following OTS-412 alone in the IT injection mouse model (Figure 3D). HU, a ribonucleotide reductase inhibitor, is currently utilized in the management of myeloproliferative disorders and sickle cell anemia.[22,34] By inducing myelosuppression, HU may aid OV to escape innate immune surveillance and keep unsought anti-viral activities from overriding anti-tumoral adaptive immunity. By a related mechanism, HU may increase stimulation of endogenous tumor-infiltrating T cells.[35,36] Beyond the

efficacy observed in the IT model, pilot studies on intravenous CAR-T injection showed synergistic effect of CAR-T following OTS-412/HU treatment (Figures S6A and S6B). Also, the coinciding infiltration of $hCD3^+$ cells with the abundant expression of A56 in tumor tissue (Figure 3E) suggests a promising outlook for the anti-tumor effect of intravenous CAR-T cell injection.

In conclusion, our study demonstrated the potency of A56 CAR-T cell therapy following OTS-412/hydroxyurea combination treatment. This was achieved through the development of A56 as a universal tumor-targeting antigen, which is expressed in tumors upon systemic OTS-412 treatment. Moreover, our results suggest the use of hydroxyurea not only as an immunomodulating agent in oncolytic virotherapy but also as a preconditioning agent to increase the specificity of A56 delivery, decreasing the likelihood of on-target/off-tumor toxicity.

Limitations of the study

In this proof-of-concept study, we focused primarily on validating A56 expression as a tumor-specific target and on conducting a preliminary assessment of the *in vitro* and *in vivo* efficacy of A56 CAR-T cells. We used a murine xenograft model for our evaluation, acknowledging its limitations. Specifically, this model is less applicable for translating findings to human systemic toxicity and constrains the comprehensive immunological assessments.[37] Concerning the safety profiles of the therapeutic agents employed, this study did not provide detailed safety data for each agent. Studies are being pursued to actively evaluate the toxicity profiles of these treatments using various modalities.[38–40] Preliminary toxicity data for OVV can, however, be inferred from a Phase I trial of Pexa-Vec, a similar construct to OTS-412, where the most frequently observed adverse events were grade 1/2 flu-like symptoms that typically resolved within 24 h.[41] Although specific safety data for HU in the context of malignancies is sparse, a long-term randomized controlled trial in sickle cell anemia patients has suggested its general safety.[42] Nonetheless, due to the limitations inherent in the present proof-of-concept study, further research is essential to clarify the safety outcomes associated with this multi-modal therapeutic approach.

STAR★METHODS

Detailed methods are provided in the online version of this paper and include the following:

- KEY RESOURCES TABLE
- RESOURCE AVAILABILITY
  - Lead contact
  - Materials availability
  - Data and code availability
- EXPERIMENTAL MODEL AND STUDY PARTICIPANT DETAILS
  - T cells and cell lines
  - *In vivo* A56 CAR-T cell efficacy studies
- METHOD DETAILS
  - Ethical statement
  - Multiple mutant A56 vector construction
  - Plasmid transfection, immunofluorescence staining, and immunohistochemistry
  - A56 expression detection by flow cytometry
  - Neutrophil co-culture experiment
  - Immunomodulatory agent screening
  - Selection of anti-A56 single-chain fragment variables containing phages
  - T cell transduction of anti-A56 CAR lentiviral vector
  - *In vitro* A56 CAR-T cells functionality assay
- QUANTIFICATION AND STATISTICAL ANALYSIS

SUPPLEMENTAL INFORMATION

Supplemental information can be found online at https://doi.org/10.1016/j.isci.2024.109256.

ACKNOWLEDGMENTS

We thank Dr. Jae Ho Kim of Pusan National University and Dr. Sang Seok Koh of Dong-A University for their review of this manuscript. This research was supported by a grant from the Korea Health Technology R&D Project through the Korea Health Industry Development Institute (KHIDI), funded by the Ministry of Health & Welfare, Republic of Korea (grant number: HI20C0523). T.H.H., M.C., and E.C. are co-inventors on a patent application covering A56 CAR-T (No. PCT/KR2021/004226).

AUTHOR CONTRIBUTIONS

Data curation, Y.S.L., E.J.R., Y.R.L., Y.J.K., C.H.L., and D.O.; writing – original draft, E.C. and M.H.A.; writing – review & editing, S.Y.P., M.S.K., N.D.K., J.-J.K., Y.M.H., M.C., and T.H.H. All authors have read and agreed to the published version of the manuscript.

DECLARATION OF INTERESTS

E.C., Y.S.L., E.J.R., Y.R.L., S.Y.P., Y.J.K., C.H.L., and D.Y.O. are currently employed at Bionoxx Inc.

Received: September 12, 2023
Revised: December 15, 2023
Accepted: February 13, 2024
Published: February 16, 2024

REFERENCES

1. Park, J.H., Rivière, I., Gonen, M., Wang, X., Sénéchal, B., Curran, K.J., Sauter, C., Wang, Y., Santomasso, B., Mead, E., et al. (2018). Long-term follow-up of CD19 CAR therapy in acute lymphoblastic leukemia. N. Engl. J. Med. *378*, 449–459. https://doi.org/10.1056/NEJMoa1709919.
2. Davila, M.L., Riviere, I., Wang, X., Bartido, S., Park, J., Curran, K., Chung, S.S., Stefanski, J., Borquez-Ojeda, O., Olszewska, M., et al. (2014). Efficacy and toxicity management of 19-28z CAR T cell therapy in B cell acute lymphoblastic leukemia. Sci. Transl. Med. *6*, 224ra25. https://doi.org/10.1126/scitranslmed.3008226.
3. Turtle, C.J., Hanafi, L.-A., Berger, C., Hudecek, M., Pender, B., Robinson, E., Hawkins, R., Chaney, C., Cherian, S., Chen, X., et al. (2016). Immunotherapy of non-Hodgkin's lymphoma with a defined ratio of CD8+ and CD4+ CD19-specific chimeric antigen receptor–modified T cells. Sci. Transl. Med. *8*, 355ra116.
4. Kochenderfer, J.N., Dudley, M.E., Kassim, S.H., Somerville, R.P.T., Carpenter, R.O., Stetler-Stevenson, M., Yang, J.C., Phan, G.Q., Hughes, M.S., Sherry, R.M., et al. (2015). Chemotherapy-refractory diffuse large B-cell lymphoma and indolent B-cell malignancies can be effectively treated with autologous T cells expressing an anti-CD19 chimeric antigen receptor. J. Clin. Oncol. *33*, 540–549. https://doi.org/10.1200/JCO.2014.56.2025.
5. Ali, S.A., Shi, V., Maric, I., Wang, M., Stroncek, D.F., Rose, J.J., Brudno, J.N., Stetler-Stevenson, M., Feldman, S.A., and Hansen, B.G. (2016). T cells expressing an anti–B-cell maturation antigen chimeric antigen receptor cause remissions of multiple myeloma. Blood J. Am. Soc. Hematol. *128*, 1688–1700. https://doi.org/10.1182/blood-2016-04-711903.
6. Fan, F., Zhao, W., Liu, J., He, A., Chen, Y., Cao, X., Yang, N., Wang, B., Zhang, P., and Zhang, Y. (2017). Durable remissions with BCMA-specific chimeric antigen receptor (CAR)-modified T cells in patients with refractory/relapsed multiple myeloma. Am. Soc. Clin. Oncol. https://doi.org/10.1200/JCO.2017.35.15_SUPPL.LBA3001.
7. Beatty, G.L., O'Hara, M.H., Lacey, S.F., Torigian, D.A., Nazimuddin, F., Chen, F., Kulikovskaya, I.M., Soulen, M.C., McGarvey, M., Nelson, A.M., et al. (2018). Activity of mesothelin-specific chimeric antigen receptor T cells against pancreatic carcinoma metastases in a phase 1 trial. Gastroenterology *155*, 29–32. https://doi.org/10.1053/j.gastro.2018.03.029.
8. Hou, B., Tang, Y., Li, W., Zeng, Q., and Chang, D. (2019). Efficiency of CAR-T therapy for treatment of solid tumor in clinical trials: a meta-analysis. Dis. Markers *2019*, 3425291. https://doi.org/10.1155/2019/3425291.
9. Bagley, S.J., and O'Rourke, D.M. (2020). Clinical investigation of CAR T cells for solid tumors: lessons learned and future directions. Pharmacol. Therapeut. *205*, 107419. https://doi.org/10.1016/j.pharmthera.2019.107419.
10. Mirzaei, H.R., Rodriguez, A., Shepphird, J., Brown, C.E., and Badie, B. (2017). Chimeric antigen receptors T cell therapy in solid tumor: challenges and clinical applications. Front. Immunol. *8*, 1850. https://doi.org/10.3389/fimmu.2017.01850.
11. Fesnak, A.D., June, C.H., and Levine, B.L. (2016). Engineered T cells: the promise and challenges of cancer immunotherapy. Nat. Rev. Cancer *16*, 566–581. https://doi.org/10.1038/nrc.2016.97.
12. Morgan, R.A., Yang, J.C., Kitano, M., Dudley, M.E., Laurencot, C.M., and Rosenberg, S.A. (2010). Case report of a serious adverse event following the administration of T cells transduced with a chimeric antigen receptor recognizing ERBB2. Mol. Ther. *18*, 843–851. https://doi.org/10.1038/mt.2010.24.
13. Lamers, C.H.J., Sleijfer, S., Vulto, A.G., Kruit, W.H.J., Kliffen, M., Debets, R., Gratama, J.W., Stoter, G., and Oosterwijk, E. (2006). Treatment of metastatic renal cell carcinoma with autologous T-lymphocytes genetically retargeted against carbonic anhydrase IX: first clinical experience. J. Clin. Oncol. *24*, e20–e22. https://doi.org/10.1200/JCO.2006.05.9964.
14. Nishio, N., and Dotti, G. (2015). Oncolytic virus expressing RANTES and IL-15 enhances function of CAR-modified T cells in solid tumors. OncoImmunology *4*, e988098. https://doi.org/10.4161/21505594.2014.988098.
15. Rosewell Shaw, A., and Suzuki, M. (2018). Oncolytic viruses partner with T-cell therapy for solid tumor treatment. Front. Immunol. *9*, 2103. https://doi.org/10.3389/fimmu.2018.02103.
16. Kaufman, H.L., Kohlhapp, F.J., and Zloza, A. (2016). Oncolytic viruses: a new class of immunotherapy drugs. Nat. Rev. Drug Discov. *15*, 660. https://doi.org/10.1038/nrd.2016.178.
17. Bommareddy, P.K., Shettigar, M., and Kaufman, H.L. (2018). Integrating oncolytic viruses in combination cancer immunotherapy. Nat. Rev. Immunol. *18*, 498–513. https://doi.org/10.1038/s41577-018-0014-6.
18. Park, A.K., Fong, Y., Kim, S.-I., Yang, J., Murad, J.P., Lu, J., Jeang, B., Chang, W.-C., Chen, N.G., Thomas, S.H., et al. (2020). Effective combination immunotherapy using oncolytic viruses to deliver CAR targets to solid tumors. Sci. Transl. Med. *12*, eaaz1863. https://doi.org/10.1126/scitranslmed.aaz1863.
19. DeHaven, B.C., Gupta, K., and Isaacs, S.N. (2011). The vaccinia virus A56 protein: a multifunctional transmembrane glycoprotein that anchors two secreted viral proteins. J. Gen. Virol. *92*, 1971–1980. https://doi.org/10.1099/vir.0.030460-0.
20. Wagenaar, T.R., Ojeda, S., and Moss, B. (2008). Vaccinia virus A56/K2 fusion regulatory protein interacts with the A16 and G9 subunits of the entry fusion complex. J. Virol. *82*, 5153–5160. https://doi.org/10.1128/jvi.00162-08.
21. Brown, C.K., Turner, P.C., and Moyer, R.W. (1991). Molecular characterization of the vaccinia virus hemagglutinin gene. J. Virol. *65*, 3598–3606. https://doi.org/10.1128/jvi.65.7.3598-3606.1991.
22. Ware, R.E., and Aygun, B. (2009). Advances in the use of hydroxyurea. Hematol. Am. Soc. Hematol. Educ. Program, 62–69. https://doi.org/10.1182/asheducation-2009.1.62.
23. Islam, S.M.B.U., Lee, B., Jiang, F., Kim, E.K., Ahn, S.C., and Hwang, T.H. (2020). Engineering and Characterization of Oncolytic Vaccinia Virus Expressing Truncated Herpes Simplex Virus Thymidine Kinase. Cancers *12*, 228. https://doi.org/10.3390/cancers12010228.
24. Liu, Z., Ravindranathan, R., Kalinski, P., Guo, Z.S., and Bartlett, D.L. (2017). Rational combination of oncolytic vaccinia virus and PD-L1 blockade works synergistically to enhance therapeutic efficacy. Nat. Commun. *8*, 14754. https://doi.org/10.1038/ncomms14754.
25. Kim, J.H., Oh, J.Y., Park, B.H., Lee, D.E., Kim, J.S., Park, H.E., Roh, M.S., Je, J.E., Yoon, J.H., Thorne, S.H., et al. (2006). Systemic armed oncolytic and immunologic therapy for cancer with JX-594, a targeted poxvirus expressing GM-CSF. Mol. Ther. *14*, 361–370. https://doi.org/10.1016/j.ymthe.2006.05.008.
26. Adams, M.M., Rice, A.D., and Moyer, R.W. (2007). Rabbitpox virus and vaccinia virus infection of rabbits as a model for human smallpox. J. Virol. *81*, 11084–11095. https://doi.org/10.1128/jvi.00423-07.
27. Jarahian, M., Fiedler, M., Cohnen, A., Djandji, D., Hämmerling, G.J., Gati, C., Cerwenka, A., Turner, P.C., Moyer, R.W., Watzl, C., et al. (2011). Modulation of NKp30- and NKp46-Mediated Natural Killer Cell Responses by Poxviral Hemagglutinin. PLoS Pathog. *7*, e1002195. https://doi.org/10.1371/journal.ppat.1002195.
28. Johnson, B.F., Kanatani, Y., Fujii, T., Saito, T., Yokote, H., and Smith, G.L. (2011). Serological responses in humans to the smallpox vaccine LC16m8. J. Gen. Virol. *92*, 2405–2410. https://doi.org/10.1099/vir.0.034207-0.
29. Walsh, S.R., Gillis, J., Peters, B., Mothé, B.R., Sidney, J., Sette, A., and Johnson, R.P. (2009). Diverse recognition of conserved orthopoxvirus CD8+ T cell epitopes in vaccinated rhesus macaques. Vaccine *27*, 4990–5000. https://doi.org/10.1016/j.vaccine.2009.05.077.

30. Pütz, M.M., Midgley, C.M., Law, M., and Smith, G.L. (2006). Quantification of antibody responses against multiple antigens of the two infectious forms of Vaccinia virus provides a benchmark for smallpox vaccination. Nat Med *12*, 1310–1315. https://doi.org/10.1038/nm1457.
31. Abreu, T.R., Fonseca, N.A., Gonçalves, N., and Moreira, J.N. (2020). Current challenges and emerging opportunities of CAR-T cell therapies. J Control Release *319*, 246–261. https://doi.org/10.1016/j.jconrel.2019.12.047.
32. Xiong, W., Chen, Y., Kang, X., Chen, Z., Zheng, P., Hsu, Y.H., Jang, J.H., Qin, L., Liu, H., Dotti, G., and Liu, D. (2018). Immunological Synapse Predicts Effectiveness of Chimeric Antigen Receptor Cells. Mol. Ther. *26*, 963–975. https://doi.org/10.1016/j.ymthe.2018.01.020.
33. Yanguas, A., Garasa, S., Teijeira, Á., Aubá, C., Melero, I., and Rouzaut, A. (2018). ICAM-1-LFA-1 Dependent CD8+ T-Lymphocyte Aggregation in Tumor Tissue Prevents Recirculation to Draining Lymph Nodes. Front. Immunol. *9*, 2084. https://doi.org/10.3389/fimmu.2018.02084.
34. Madaan, K., Kaushik, D., and Verma, T. (2012). Hydroxyurea: a key player in cancer chemotherapy. Expert Rev. Anticancer Ther. *12*, 19–29. https://doi.org/10.1586/era.11.175.
35. Aarts, C.E.M., Hiemstra, I.H., Béguin, E.P., Hoogendijk, A.J., Bouchmal, S., van Houdt, M., Tool, A.T.J., Mul, E., Jansen, M.H., Janssen, H., et al. (2019). Activated neutrophils exert myeloid-derived suppressor cell activity damaging T cells beyond repair. Blood Adv. *3*, 3562–3574. https://doi.org/10.1182/bloodadvances.2019031609.
36. Wang, T.T., Zhao, Y.L., Peng, L.S., Chen, N., Chen, W., Lv, Y.P., Mao, F.Y., Zhang, J.Y., Cheng, P., Teng, Y.S., et al. (2017). Tumour-activated neutrophils in gastric cancer foster immune suppression and disease progression through GM-CSF-PD-L1 pathway. Gut *66*, 1900–1911. https://doi.org/10.1136/gutjnl-2016-313075.
37. Duncan, B.B., Dunbar, C.E., and Ishii, K. (2022). Applying a clinical lens to animal models of CAR-T cell therapies. Mol. Ther. Methods Clin. Dev. *27*, 17–31. https://doi.org/10.1016/j.omtm.2022.08.008.
38. Valiullina, A.K., Zmievskaya, E.A., Ganeeva, I.A., Zhuravleva, M.N., Garanina, E.E., Rizvanov, A.A., Petukhov, A.V., and Bulatov, E.R. (2023). Evaluation of CAR-T Cells' Cytotoxicity against Modified Solid Tumor Cell Lines. Biomedicines *11*, 626. https://doi.org/10.3390/biomedicines11020626.
39. Liu, D., and Zhao, J. (2018). Cytokine release syndrome: grading, modeling, and new therapy. J. Hematol. Oncol. *11*, 121. https://doi.org/10.1186/s13045-018-0653-x.
40. Nouri, Y., Weinkove, R., and Perret, R. (2023). An In Vitro Model to Assess CRS Potential of CAR T Cells Using a Tumor Cell Line and Autologous Monocytes. Curr. Protoc. *3*, e864. https://doi.org/10.1002/cpz1.864.
41. Park, S.H., Breitbach, C.J., Lee, J., Park, J.O., Lim, H.Y., Kang, W.K., Moon, A., Mun, J.-H., Sommermann, E.M., Maruri Avidal, L., et al. (2015). Phase 1b Trial of Biweekly Intravenous Pexa-Vec (JX-594), an Oncolytic and Immunotherapeutic Vaccinia Virus in Colorectal Cancer. Mol. Ther. *23*, 1532–1540. https://doi.org/10.1038/mt.2015.109.
42. Steinberg, M.H., McCarthy, W.F., Castro, O., Ballas, S.K., Armstrong, F.D., Smith, W., Ataga, K., Swerdlow, P., Kutlar, A., DeCastro, L., and Waclawiw, M.A.; Investigators of the Multicenter Study of Hydroxyurea in Sickle Cell Anemia and MSH Patients' Follow-Up (2010). The risks and benefits of long-term use of hydroxyurea in sickle cell anemia: A 17.5 year follow-up. Am. J. Hematol. *85*, 403–408. https://doi.org/10.1002/ajh.21699.
43. Paugh, B.S., Baranyi, L., Roy, A., He, H.-J., Harris, L., Cole, K.D., Artlip, M., Raimund, C., Langan, P.S., Jana, S., et al. (2021). Reference standards for accurate validation and optimization of assays that determine integrated lentiviral vector copy number in transduced cells. Sci. Rep. *11*, 389. https://doi.org/10.1038/s41598-020-79698-w.
44. Saad, N.S., Floyd, K., Ahmed, A.A.E., Mohler, P.J., Janssen, P.M.L., and Elnakish, M.T. (2016). The Effect of Sorafenib, Tadalafil and Macitentan Treatments on Thyroxin-Induced Hemodynamic Changes and Cardiac Abnormalities. PLoS One *11*, e0153694. https://doi.org/10.1371/journal.pone.0153694.
45. Jinesh G, G., Lee, E.K., Tran, J., and Kamat, A.M. (2013). Lenalidomide augments the efficacy of bacillus Calmette-Guerin (BCG) immunotherapy *in vivo*. Urol. Oncol. Semin. Original Invest. *31*, 1676–1682. https://doi.org/10.1016/j.urolonc.2012.05.007.

STAR★METHODS

KEY RESOURCES TABLE

REAGENT or RESOURCE	SOURCE	IDENTIFIER
Antibodies		
Anti-A56 antibody	Immune Technology	Cat# IT-012-006M1
Anti-A27 antibody	Santa Cruz	Cat# SC-69950; RRID: AB_1131166
Alexa 488 secondary antibody	Thermo-Fisher Scientific	Cat# A21204; RRID: AB_2535790
CD25 Monoclonal Antibody (CD25-4E3), APC	ebioscience	Cat# 17-0257-42; RRID: AB_11218671
CD3 Monoclonal Antibody (SK7), APC	ebioscience	Cat# 11-0036-42; RRID: AB_1272072
Human CD3 polyclonal antibody, Unconjugated	Agilent Technologies	Cat# A045229
Dako REAL Encision/HRP	Dako	Cat# K5007
Alexa Fluor 647 Goat Anti-Mouse IgG H&L	Abcam	Cat# ab150115; RRID: AB_2687948
PI-Live/dead staining antibody	BD Biosciences	Cat# 556547; RRID: AB_2869082
APC anti-His Tag Antibody	BioLegend	Cat# 362605; RRID: AB_2715828
Zombie Aqua™ Fixable Viability Kit	BioLegend	Cat# 423102
Bacterial and virus strains		
OTS-412 recombinant vaccinia virus	Bionoxx	N/A
WR VV^{tk-}	Bionoxx	N/A
XL1-Blue competent cells	Agilent	Cat# 200249
Biological samples		
Human peripheral blood	Isolated from healthy donors	IRB# 05-2019-095
Chemicals, peptides, and recombinant proteins		
BamH1 enzyme	Thermo-Fisher Scientific	Cat# ER0051
CellLight-ER-RFP	Thermo-Fisher Scientific	Cat# C10591
CellLight-Golgi-RFP	Thermo-Fisher Scientific	Cat# C10593
Cytotox Red reagent	EssenBioscience	Cat# 4632
Dulbecco's phosphate-buffered saline	Wellgene	Cat# LB001-02
FastDigest Xho1 enzyme	Thermo-Fisher Scientific	Cat# FD0694
Fetal Bovine Serum	Hyclone/Cytiva	Cat# SH30071.03
Ficoll-Paque PLUS	GE Healthcare	Cat# GE17-1440-03
Formalin	VWR	Cat# VWRU89370-094
Glycine	Biorad	Cat# 1610717
Hematoxylin	MUTO	Cat# 30002
hFc/mFc-tagged A56 protein	This paper	N/A
His-tagged A56 protein	This paper	N/A
Hydroxyurea	Sigma	Cat# 127-07-1
Intracellular Fixation & Permeabilization Buffer	ebioscience	Cat# 88-8824-00
polyethylenimine	Aldrich	Cat# 408727
Recombinant human IL-2	Miltenyi Biotec	Cat# 130-097-748
RPMI 1640	Hyclone/Cytiva	Cat# SH30027.01
T cell TransAct™, human	Miltenyi Biotec	Cat# 130-111-160
TexMACS medium	Miltenyi Biotec	Cat# 130-097-196
TheraPEAK™ ACK Lysing Buffer (1x)	Lonza	Cat# BP10-548E

(*Continued on next page*)

Continued

REAGENT or RESOURCE	SOURCE	IDENTIFIER
Tris, acetate, EDTA (TAE) buffer	Invitrogen	Cat# 15558026
Tryple select	Gibco	Cat# 12563029
Tween 20	Sigma	Cat# 1702
CellLight-ER-RFP	Thermo-Fisher Scientific	Cat# C10591
Trimidox	Cayman Chemical	Cat# 10009083
Didox	Sigma	Cat# 69839-83-4
Tadalafil	Cayman Chemical	Cat# 14024
Lenalidomide	NATCO	Cat# 602539
Cyclophosphamide	Sigma	Cat# C0768
Critical commercial assays		
Vector Mouse-on-Mouse Kit	Vector Laboratories	Cat# FMK-2201
Pan T cell isolation kit, human	Miltenyi Biotec	Cat# 130-096-535
Experimental models: Cell lines		
HT-29 cells	KCLB	Cat# 30038
HCT-116 cells	KCLB	Cat# 10247
A549 cells	ATCC	Cat# CCL-185
HeLa cells	ATCC	Cat# CCL-2
SK-MEL-5 cells	KCLB	Cat# 30070
PC-3 cells	KCLB	Cat# 21435
MCF-7 cells	KCLB	Cat# 30022
U-2 OS cells	ATCC	Cat# HTB 96
HEK293F cells	Y-Biologics Inc.	N/A
Experimental models: Organisms/strains		
Mouse: NOD.CB17-Prkdcsscid/NCrKoat	KOATECH	N/A
Rabbit: New Zealand White Rabbit/ Oryctolagus Cuniculus	Samtako/Hanabio	N/A
Oligonucleotides		
N293F expression vector	Y-Biologics Inc.	N/A
A56-F primer	This paper	N/A
A56-R primer	This paper	N/A
pcDNA3.1-cFLAG vector	Y-Biologics Inc.	N/A
Recombinant DNA		
Lentiviral vector	Miltenyi Bioindustry	N/A
Software and algorithms		
FLUOVIEW FV10-ASW 4.2 software	Olympus	N/A
Kaluza Analysis v.2.1	Beckman Coulter	Cat# B16407
GraphPad Prism v.8.4.2	GraphPad	N/A
MoFlo Astrios EQ, Cell Sorter Summit V6.3.1.16945	Beckman Coulter	N/A
IncuCyte S3 Live-Cell Analysis System	Sartorius	N/A
Other		
BD Vacutainer® K2E(EDTA)	BD	Cat# 367525

RESOURCE AVAILABILITY

Lead contact

Further information and requests for resources and reagents should be directed to and will be fulfilled by the lead contact, Tae Ho Hwang (thhwang@pusan.ac.kr).

Materials availability

Unique reagents generated in this study include anti-A56 antibodies, A56 CAR-T cells and OTS-412 recombinant vaccinia virus. There are restrictions to the availability of these reagents as they have been patented and will be made available only for research purposes under a material transfer agreement through Bionoxx Inc.

Data and code availability

- The data reported in this study cannot be deposited in a public repository because the data are proprietary.
- This paper does not report original code.
- Any additional information required to reanalyze the data reported in this paper is available from the lead contact upon request.

EXPERIMENTAL MODEL AND STUDY PARTICIPANT DETAILS

T cells and cell lines

Peripheral blood was obtained from healthy donors with the approval of the Institutional Review Board of Pusan National University Yangsan Hospital (Approval no. 05-2019-095). The healthy donors included Asian men(n = 6) and women(n = 5) of an age range of 23–44 years. T cells were expanded in TexMACS medium (Miltenyi Biotec, Bergisch Gladbach, DE, USA) supplemented with 10% fetal bovine serum (FBS; HyClone, Logan, UT, USA) and 20 IU/mL of recombinant human IL-2 (rhIL-2; Miltenyi Biotec). T cells were stimulated with anti-CD3 and anti-CD28 mAbs-coated particles (TransAct; Miltenyi Biotec) at a ratio of 1:1 following the manufacturer's instructions.

HCT-116 (colorectal carcinoma; KCLB, Seoul, Korea), A549 (lung carcinoma; American Type Culture Collection (ATCC), Manassas, VA, USA), HT-29 (colorectal carcinoma; KCLB, Seoul Korea), PC-3 (prostate adenocarcinoma; KCLB, Seoul, Korea), MCF-7 (breast adenocarcinoma, KCLB, Seoul, Korea), U2-OS (osteosarcoma) human cell lines were cultured in 10% FBS-RPMI 1640 medium (HyClone). HeLa (cervical carcinoma; ATCC) and SK-MEL-5 (malignant melanoma; KCLB) human cell lines were cultured in 10% FBS-DMEM medium (HyClone). The cell lines were tested for mycoplasma and authenticated by Short Tandem Repeat analysis by their respective providers.

Informed Consent Statement: Informed consent has been obtained from the donors to publish this paper.

In vivo A56 CAR-T cell efficacy studies

Seven-week-old female NOD.SCID mice were subcutaneously injected under anesthesia with 2 x 10^6 HCT-116 cells resuspended in 100 μL of saline. All mice experiments used mice of the same species, age and sex. When the tumor volume exceeded around 100 mm^3, 30 mg/kg of hydroxyurea (HU) was injected intraperitoneally, six days a week. To assess A56 expression, 1 x 10^5, 1 x 10^6, or 1 × 10^7 pfu of OTS-412 per mouse was injected intravenously in the retro-orbital sinus 4 h after the first injection of HU. For the rabbit model, 18-20 week-old male and female New Zealand White (Oryctolagus Cuniculus) rabbits were intramuscularly injected under anesthesia with VX2 tumor cells. 1.5 × 10^7 pfu of OTS-412 per rabbit was injected into the ear vein with 60 mg/kg of HU treatment for 7 days.

For the IT model studies, HCT-116 tumor-bearing mice were administrated intraperitoneally with HU (30 mg/kg, six days a week), and 3 days post-OTS-412 injection at 1 × 10^6 pfu 2 x 10^6 CAR-positive T cells resuspended in 100 μL of saline per mouse were injected intratumorally. For intravenous model, mice were treated with HU for two weeks, and 10 days post-OTS-412 injection, 4 x 10^5 CAR-positive T cells prepared in 100 μL of saline per mouse was injected intravenously into the retro-orbital sinus. Brain, heart, lung, liver, spleen, kidney, ovary, and tumor tissue were isolated for pathological analysis by IHC. Humane endpoints (tumor volumes reaching 800 mm^3 or above) were the basis for time-to-tumor-progression (TTP).

METHOD DETAILS

Ethical statement

7-week-old Female NOD.CB17-Prkdcsscid/NcrKoat mice and BALB/c mice were purchased from KOATECH Inc (Pyeongtaek, Korea). Mice with an average of 20 g were used as a tumor model after quarantine and stabilization. General procedures for animal care and housing were conducted following the approved protocol (2021-013-A1C0(0)) by the animal care committee of PNUYH and institutional guidelines. Less than five mice per an individual ventilated cage were kept in an isolated SPF barrier room at 22 ± 2°C with 40–70% relative humidity on a 12 h light/dark cycle.

Multiple mutant A56 vector construction

The full A56 gene sequence with a green fluorescence protein (GFP) at the N-terminus was inserted into a pcDNA3.1 (Thermo-Fisher Scientific, Massachusetts, USA) vector by overlapping PCR amplification. Additional overlapping PCR was performed to delete each domain from

the full-length A56 vector using specific primers. Then, each PCR product was cloned into a pcDNA3.1 vector using BamH1 and FastDigest Xho1 enzymes (Thermo-Fisher Scientific). For, anti-A56 scFv vector construction, anti-A56 scFv sequences obtained from human phage library selection were each fused with a human CD8α transmembrane domain and 4-1BB and CD3ζ stimulatory domains and incorporated into a lentiviral vector (Miltenyi Bioindustry, Gaithersburg, MD, USA) by transient transfection of a transfer construct and three packaging helper plasmids into 293T cells in a suspension system.[43]

Plasmid transfection, immunofluorescence staining, and immunohistochemistry

U2-OS cells were cultured overnight on Cellview slides (Greiner Bio-One, Chonburi Thailand), containing 10 round wells matching the plate design of a standard 96-well, and the cells were transfected with 0.25 μg/well of GFP-tagged A56 or GFP-tagged A56 mutant plasmids using Xfect transfection reagent (Takara Bio, San Jose, USA) in serum-free conditions. After 4 h of transfection, the cells were washed and supplemented with fresh growth medium. For cellular organelles, the cells were treated with CellLight-Golgi-RFP or CellLight-ER-RFP (Thermo-Fisher Scientific) 24 h post-transfection and incubated at 37°C overnight. Forty-eight hours post-transfection, the cells were fixed with 4% paraformaldehyde at 4°C for 10 min and rinsed with PBS. To visualize the nuclei, the cells were stained with 4′-6-diamidino-2-phenylindole for 1 min at room temperature and then washed twice with PBS. Immunohistochemistry (IHC) was performed on paraffin-embedded sections stained with anti-A56 (Immune Technology, New York, NY, USA; 1:200) or anti-A27L antibody (Antibodies-Online, Aachen, Germany; 1:200). The secondary antibody used was Alexa 488 (Thermo-Fisher Scientific; 1:200). For IHC of mouse tissue, the Vector Mouse-on-Mouse Kit (M.O.M., Vector Laboratories, Burlingame, CA, USA) was used according to the manufacturer's instructions. Cells and tissue sections were visualized using a Nikon fluorescent microscope and a confocal microscope (OLYMPUS, FV1000) using FLUOVIEW FV10-ASW 4.2 software.

A56 expression detection by flow cytometry

To determine expression of A56 along with the quantification of cell viability, various tumor cells were seeded onto 6-well plates in DMEM or RPMI 1640 supplemented with 10% FBS. Next day, the cells were infected with 0, 0.0125, 0.025, 0.05, 0.1, and 1 MOI of OTS-412 for 2, 24, and 48 h. At the specified time, the cells were harvested and stained with Fixable Viability Dye Zombie Aqua (BioLegend, San Diego, CA, USA) for 20 min at room temperature in the dark to exclude dead cells. For A56 detection on the plasma membrane, the cells were labeled with 1μg of anti-A56 antibody (Mouse IgG1 w/o kappa light chain) (LakePharma, Variant 3) diluted in PBS supplemented with 2% FBS for 30 min at 4°C. Sequentially, the cells were rinsed and stained with goat anti-Mouse IgG H&L Alexa Fluor 647 conjugated antibody (1:1000 dilutions) (Abcam, HK) for 30 min at 4°C in the dark. For intracellular A56 detection, fixation/permeabilization was performed with an Intracellular Fixation & Permeabilization Buffer Set (eBioscience) according to the manufacturer's instruction. Then, the pellets were stained in the same manner as the surface A56 detection. Experiments were conducted on Moflo Astrios flow cytometer (Beckman Coulter, Istanbul, Turkey) and analyzed by Kaluza software v2.2.

Neutrophil co-culture experiment

HT-29 cancer cells were seeded at 2×10^5 cells/well in the Transwell 24-well plates (Corning Life Sciences, AZ, USA) in 10% FBS-RPMI 1640. On day 1, after infection with 0.3 MOI of OTS-412 for 2 h in 2% FBS-media, the infection media were changed to the growth media. After 24 h incubation, 1×10^4, 1×10^5, 1×10^6 concentrations of isolated human neutrophils were seeded into a transwell insert, which was layered onto the infected cells. After 24 h of co-culture quantification of live/dead cancer cells was determined with PI/Annexin V staining using Moflo Astrios flow cytometer (Beckman Coulter, Istanbul, Turkey) and analyzed by Kaluza software v2.2.

Immunomodulatory agent screening

Eight-week-old, female BALB/c mice were subcutaneously injected under anesthesia with 5×10^6 Renca cells resuspended in 100 μL of saline. When the tumor volume reached approximately 80–100 mm^3, WR VV^{tk-} virus (western reserve strain-derived oncolytic vaccinia virus with thymidine kinase gene deletion) was injected once intraperitoneally (IP) at 1×10^7 pfu/200 μL/mice. Immunomodulatory agents or ribonucleotide reductase inhibitors were injected as follows: Tadalafil – 4 mg/kg,[44] PO, 6 days; Lenalidomide – 30 mg/kg,[45] PO, 6 days; HU – 30 mg/kg, IP, 5 or 6 days; Trimidox – 50 mg/kg, IP, 5 days; Didox – 125 mg/kg, IP, 5 days, Cyclophosphamide – 30 mg/kg, IP, 6 days.

Selection of anti-A56 single-chain fragment variables containing phages

The extracellular domain sequence of A56 was cloned into an N293F expression vector by polymerase chain reaction (PCR) using an A56-F primer (5′-ACACCTTTTCCTCAGACATC-3′) and an A56-R primer (5′-TTCTACAAAGTCCTTGG-3′). A56 encoding the N293F expression vector and polyethyleneimine (PEI, Sigma-Aldrich, St. Louis, USA) polyplex were transfected into HEK-293 cells and incubated for 6 days. The proteins were then purified by affinity chromatography using protein A agarose (Bio Basic, Markham ON, Canada) for hFc/mFc-tagged A56 and nickel-charged nitrilotriacetic (Ni-NTA) biosensors (ForteBIO, California, USA) for his-tagged A56. The proteins were washed with 1X phosphate-buffered saline (PBS, pH 7.4) several times, and 0.1 M glycine (pH 3.3) was used for protein elution. The eluted samples were concentrated twice using AmiconR Ultra Centrifugal Filters (Millipore, Burlington, MA, USA), and resuspended in PBS. Bio-panning of phage-binding to the synthesized A56 proteins was performed using a human cDNA phage library. In summary, purified A56 proteins with >90% purity were coated on immune tubes or beads, incubated at room temperature for 1 h, washed with PBS mixed with Tween 20 (PBS/T), then Dulbecco's phosphate-buffered saline (DPBS, Wellgene, Korea), incubated with 100 mM Tris, acetate, EDTA (TAE) buffer in

dH2O, and further incubated with XL1Blue competent cells (Agilent Technologies, Santa Clara, CA, USA) at 37°C for 1 h. Three rounds of bio-panning were performed to acquire high binding affinity phages.

T cell transduction of anti-A56 CAR lentiviral vector

Human normal peripheral blood mononuclear cells (PBMCs) were isolated by Ficoll-Paque (GE Healthcare, Chicago, USA, density = 1.077 g/mL, #GE17-1440-03) density gradient separation using the SepMate system (StemCell, Seoul, Korea, #86450). T cells negatively selected by magnetic cell sorting were activated with TransAct (Miltenyi Biotec, Seoul, Korea, #130-111-160) in 10% FBS-TexMACS medium (Miltenyi Biotec, #130-097-196) supplemented with 20 IU/mL of rhIL-2 (Miltenyi Biotec, #130-097-748). To increase the yield of CAR-positive cells, T cells were transduced with 20 MOI of lentivirus containing anti-A56 CAR constructs on a rocker (FINEPCR, CR300) for 24 h following activation. T cells were maintained at a density of 1 x 10^6 cells per mL per cm^2 and incubated until day 12 at 37°C and 5% CO_2.

In vitro A56 CAR-T cells functionality assay

For the A56 CAR-T cell real-time cytotoxicity assay, various target cells were seeded onto ImageLock 96-well plates in 10% FBS-DMEM or 10% FBS-RPMI 1640. On day 1, after infection with 0.05 MOI of OTS-412 for 2 h in 2% FBS-media, the infection media were changed to 10% FBS-TexMACS. Then, the cells were incubated additional 4 h. A56 CAR-T cells (E:T = 3:1) were co-cultured at 6 h post infection. To enable the detection of tumor cell lysis using the IncuCyte live-cell analysis system (Sartorius, Gyeonggi-do, Korea), Cytotox Red Reagent (EssenBioscience, Michigan, USA, #4632) was added to each well. The plates were placed inside an IncuCyte to monitor red fluorescence at 10× magnification at three distinct locations per well, every 5 min for 6 h for 5 days. Quantification of the lysed cells was determined using the total red object area (μm^2/image) metric. Each condition was performed in duplicate or triplicate.

For the A56 CAR-T cell activation assay, various target cells were seeded onto 12 well-plates. Next day, after infection with 1 MOI of OTS-412 for 2 h in 2% FBS-media, the infection media were changed to 10% FBS- TexMACS. Then the cells incubated for additional 4 h. A56 CAR-T cells (E:T = 1:1) were co-cultured at 6 h post infection. After 24 h, the cells were harvested and excluded dead population by staining with Zombie Aqua. Sequentially, the cells were labeled with surface antibodies against CD3 (clone 17A2) and CD25 (clone CD25-4E3) in the same manner as A56 expression detection by flow cytometry.

QUANTIFICATION AND STATISTICAL ANALYSIS

The localization of A56 on solid tumor plasma membrane and the cytotoxicity tests on various cancer cell lines are presented as mean values ± SEM. Two-tailed unpaired t-test was used to determine differences in cytotoxicity between UTD-T and A56 CAR-T cells. The data for *in vivo* functionality of A56-specific A56 CAR-T cells are represented as the mean ± SD. Two-way ANOVA followed by the Tukey test was used to assess differences in tumor volume between multiple treatment groups at different time points. The two-tailed unpaired t-test was used to compare $hCD3^+$ cell quantities between UTD-T and A56 CAR-T cell treatment groups. The Kaplan-Meier estimate with log rank (Mantel-cox) test was used for time-to-tumor progression analysis. P-values of <0.05 were considered statistically significant. All statistical analyses were performed using Prism v.8.4.2 software (GraphPad, La Jolla, CA, USA).